

Exposure to precipitation from tropical cyclones has increased over the continental United States from 1948 to 2019

Laiyin Zhu ¹ & Steven M. Quiring ² 

Extreme precipitation from tropical cyclones can generate large-scale inland flooding and cause substantial damage. Here, we quantify spatiotemporal changes in population risk and exposure to tropical cyclone precipitation in the continental eastern United States over the period 1948–2019 using high-resolution in-situ precipitation observations. We find significant increases in the magnitude and likelihood of these extreme events due to increased rainfall rates and reduced translation speeds of tropical cyclones over land. We then develop a social exposure index to quantify exposure and risk of tropical cyclone precipitation as a function of both physical risk and socio-economic activities. Increased social exposure is primarily due to the increased risk of tropical cyclone precipitation, but there are regional differences. We identify exposure hotspots in the south-eastern United States, where rapid population growth and economic development amplify societal exposure to tropical cyclone hazards. Our multi-scale evaluation framework can help identify locations that should be targeted for mitigation and adaptation activities to increase their climate resilience.

¹ Department of Geography, Environment, and Tourism, Western Michigan University, Kalamazoo, MI, USA. ² Atmospheric Sciences Program, Department of Geography, The Ohio State University, Columbus, OH, USA. email: quiring.10@osu.edu

Extreme precipitation from Tropical Cyclones (TC) can cause significant inland flooding in both coastal and interior areas in the continental U.S. (CONUS) and lead to substantial economic damage. For example, Hurricane Harvey (2017) caused \$136.7 billion in losses, mostly from rain-induced inland flooding¹. It ranks as the second most expensive disaster after Hurricane Katrina. Similar flooding disasters also occurred in Hurricane Irene (2011), Hurricane Florence (2018), and Hurricane Ida (2021). Tropical Cyclone Precipitation (TCP) will likely increase in the future because a warming climate will increase TC rain rate and reduce TC translation speed^{2–4}, causing more frequent stalling⁵. These changes in TCP patterns will elevate inland flooding risk⁶. In addition, local factors such as the urban heat island effect⁷ and aerosols⁸ can further exacerbate risk by intensifying TCP.

While the physical risk of TCP is changing, there have also been substantial shifts in regional demographics and economic development. These changes are likely to continue in the future⁹. Therefore, inflation-adjusted GDP is an essential criterion to quantify historical^{10–13} and future trends¹⁴ in TC damages. Two studies^{10,15} have concluded that there is no trend in destruction because of the lack of trends in landfalling TC frequency and intensity¹³ in CONUS. In contrast, Klotzbach et al.¹¹ used a more extended period of record and found positive trends in hurricane-related economic losses in CONUS. In addition, there are also observed increases in socio-economic exposure globally and regionally¹⁶ from TC wind damages^{11,14,17}. While many discussions have focused on damages caused from TC winds, few^{10,18} have focused on impacts from TCP and inland flooding. In a changing climate, local mitigation, adaptation, and risk management are crucial for reducing the effects of TCs¹⁹. Here we use a long-term, high-resolution TCP record (at 0.25°) derived from daily in-situ precipitation observations²⁰, high-resolution population data (highest resolution of 1 km)²¹ and Gross Domestic Product (GDP, 1 km)²² to quantify spatial and temporal changes in physical TCP risk and socio-economic exposure to TCP in CONUS over 70 years (1949 to 2018). We summarize changes at the local, state, and national levels to inform mitigation and adaptation strategies.

Results

Temporal trends in TCP. About 3.7 million km² (30%) of CONUS has consistent TCP records from 1949 to 2018 (Fig. 1a) and 52,000 km² (0.4% of CONUS) has a statistically significant positive trend in annual TCP. There is an even larger area (144,000 km², 1.2% of CONUS) that has a statistically significant positive trend in annual maximum event TCP (Fig. 1b). There is also small area with negative trend (~28,000 km² for annual TCP and 1540 km² for annual maximum event TCP), although not statistically significant. Most locations with increasing annual TCP trends are located in the mid-Atlantic and south-eastern Atlantic coast (Fig. 1a). In comparison, extreme TCP (Fig. 1b) has a more expansive spatial pattern with significant positive trends in the northeastern Atlantic coast, Gulf coast, and some inland locations. There are different spatial patterns for increases in daily rain rate (Supplementary Fig. 2), annual TCP days (Supplementary Fig. 3) and durations of TCP events (Supplementary Fig. 4) and they all contribute to increases in total and extreme TC in Fig. 1. Previous studies have found either positive trends in TCP^{23–26} or no trend in TCP^{27,28} over CONUS. Differences in the length of the record, the definition of the TCP (radius to the TC center), or the source of rainfall data are possible causes of the lack of agreement in past studies. Our novel dataset shows that there is substantial spatial variability in annual total and extreme TCP trends. The mainly positive trends are caused by increased TC rain rate and event duration.

Changes in TCP Probability. We have chosen 100 and 200 mm as the thresholds to quantify changes in the Return Periods (RP) of extreme TCP events across the CONUS because 100 mm is a general precipitation threshold for generating flooding²⁹ and 200 mm indicates an extreme precipitation event^{30,31}. The RPs are calculated for two overlapping 50-year time windows (Fig. 2) to evaluate changes between the early period (1949 to 1998) and the late period (1969–2018). The overlapping period of record was selected so that we are using a robust and conservative estimate of changes in return periods for extreme events. Please see the “Methods” and Supplementary Fig. 10 for results of the sensitivity analysis using non-overlapping periods. Only 529,760 km² of areas in CONUS have <25 years RP for >100 mm event TCP in the early period (Fig. 2a), and it increases to 904,750 km² in the late period (Fig. 2b) with a relative increase of 70%. The >200 mm TCP (Fig. 2c, d) events are rarer but more destructive. We observe a ten-fold increase in the areas with <25 years RP from 11,550 km² in the early period to 117,810 km² in the late period. Geographically, locations with a higher risk of extreme TCP are mostly in coastal areas during the early period, but these higher-risk regions extend much further inland during the later period (Fig. 2b, d).

Cities have concentrations of people and economic activities, so they usually have greater exposure to extreme weather hazards³². Rapid urbanization and elevated risk of severe weather jointly exacerbate the damage risk^{33,34}. Therefore, we chose nine large cities (locations shown as Supplementary Fig. 5) along the coast for analysis, and many have increased TCP risk (Fig. 3). Houston has the most significant increase, with the 20-year event TCP increased from <200 mm in the early period to >400 mm in the late period. The tail of the distribution during the late period increases to > 600 mm as a result of extreme events like Tropical Storm Alison (2001), Hurricane Ike (2008), and Harvey (2017) in the late period. Other large cities, including New Orleans, Mobile, Tampa, Jacksonville, and Raleigh, have also experienced substantial increases in TCP risk (Fig. 3b–f). Cities further to the north generally have lower TCP risk and demonstrate different patterns of change in TCP risk. For example, TCP risk increased by 50% in New York City and decreased slightly in Boston, while it did not change in Washington, D.C. This is partly a function of the uncertainties in determining TCP risk in regions that experience fewer TCs.

TC rain rate generally follows the Clausius–Clapeyron equation, and many previous studies have demonstrated that higher global mean atmospheric temperature will lead to more precipitation^{2,35,36}. Our analysis shows substantial increases in TC rain rates over CONUS during the last 70 years (Supplementary Figs. 2, 6) and increased probabilities of higher rain rates in many major cities (Supplementary Fig. 7). At the same time, the mean translation speed of TCs decreased from 10.55 kt in the early period to 10.37 kt (Supplementary Fig. 8) in the late period (~1.7%). This reduction is most pronounced in the distribution's 0 to 20 kt range. We also find high spatial variability in changes in TC translation speeds, and clustered grids with slowing downs are in the southern part of CONUS (Supplementary Fig. 9). There is still debate on the global trend in TC translation speed^{37–39}. Nevertheless, our records indicate that the recent increase in TCP risk in CONUS is associated with a substantial rise in TC rain rate and a slight decrease in regional TC translation speed over land.

Changes in socio-economic exposure to TCP. In CONUS, substantial demographic and economic changes have occurred in the last 70 years. For example, the southern “Sunbelt” population has increased since 1950, driven by economic growth, demand for amenities, and housing supply⁴⁰. Meanwhile, these locations are

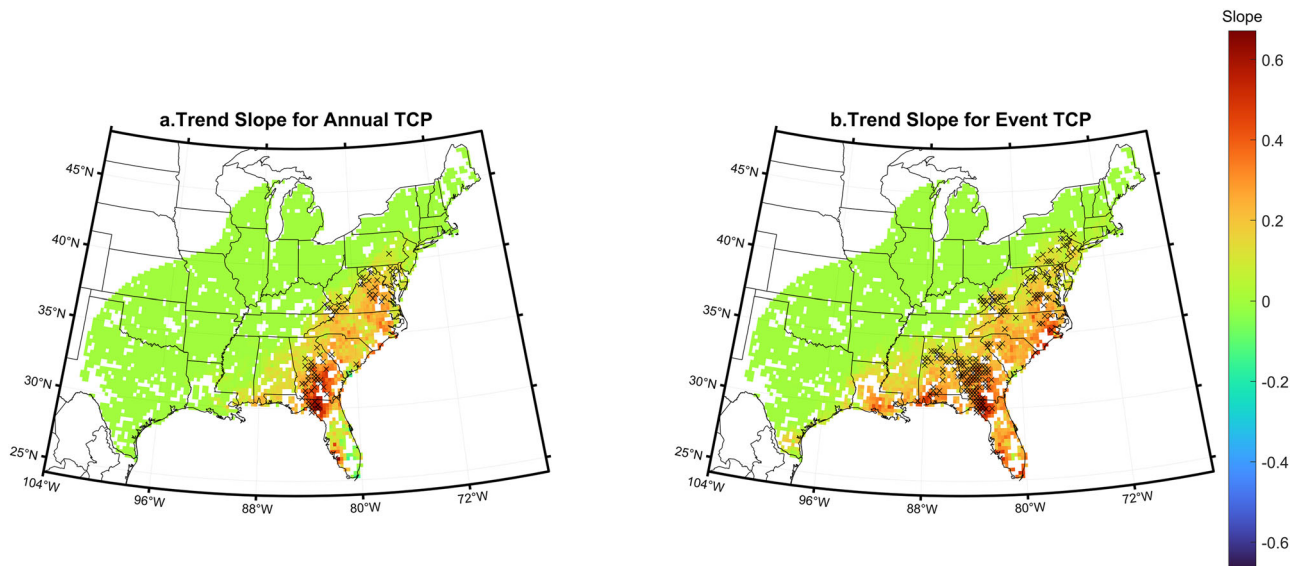


Fig. 1 Trends in tropical cyclone precipitation from 1949 to 2018 in CONUS. The trend at each location is calculated using Sen’s slope (mm year⁻¹) for: **a** annual total Tropical Cyclone Precipitation (TCP), and **b** annual maximum event TCP from 1949 to 2018 in CONUS. Black dot indicates that the trend at that location is statistically significant based on the Mann-Kendal test at the 95% significance level.

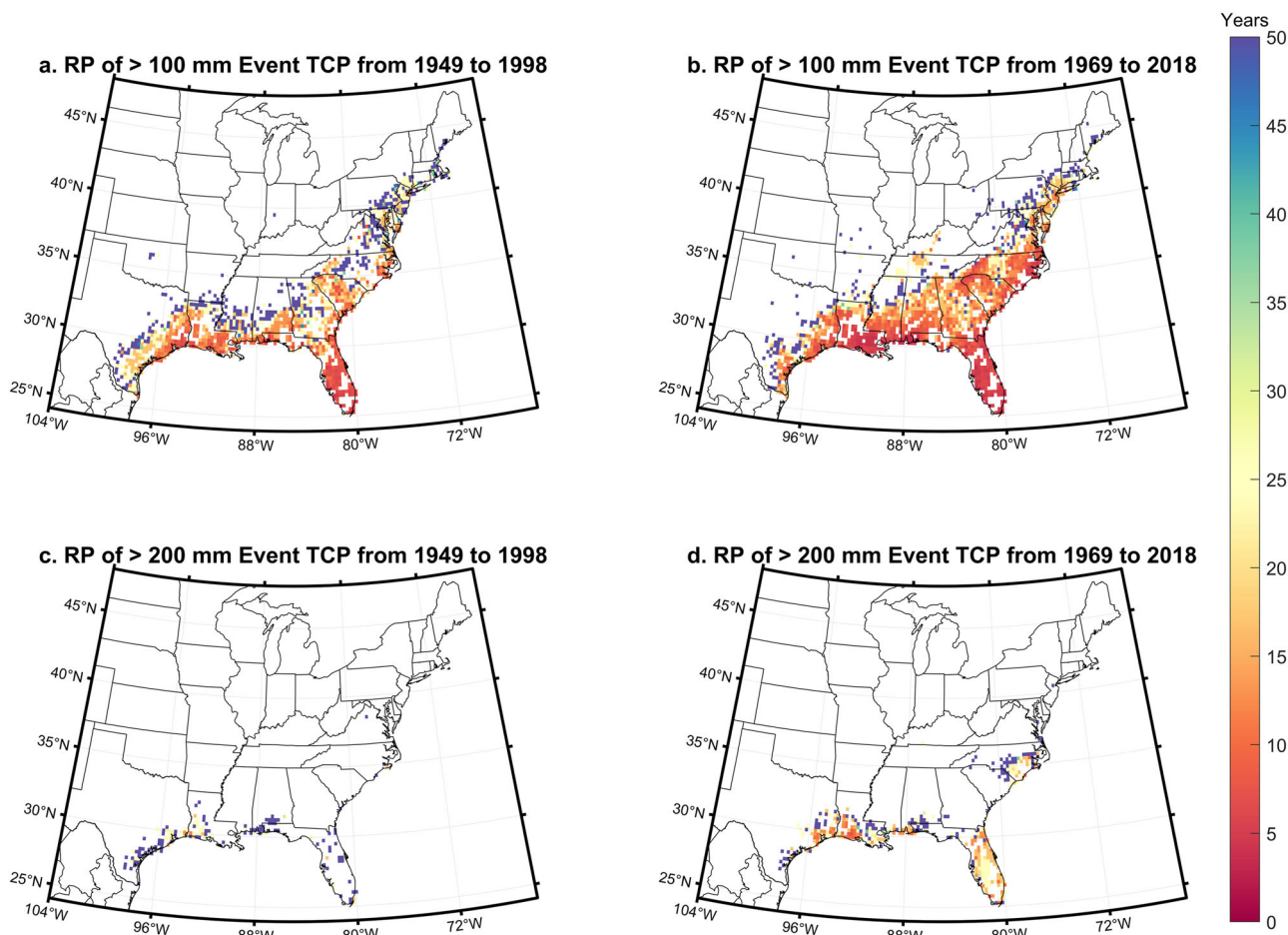


Fig. 2 Comparison of Return Period (RP, in years) for 100 and 200 mm Tropical Cyclone Precipitation (TCP) events between the early period (1949–1998) and the late period (1960 to 2018). Each panel is **a** RP for 100 mm TCP events in the early period, **b** RP for 100 mm TCP events in the late period, **c** RP for 200 mm TCP events in the early period and, **d** RP for 100 mm TCP events in the late period. Only locations with robust estimation of the empirical exceedance probability density curve are displayed.

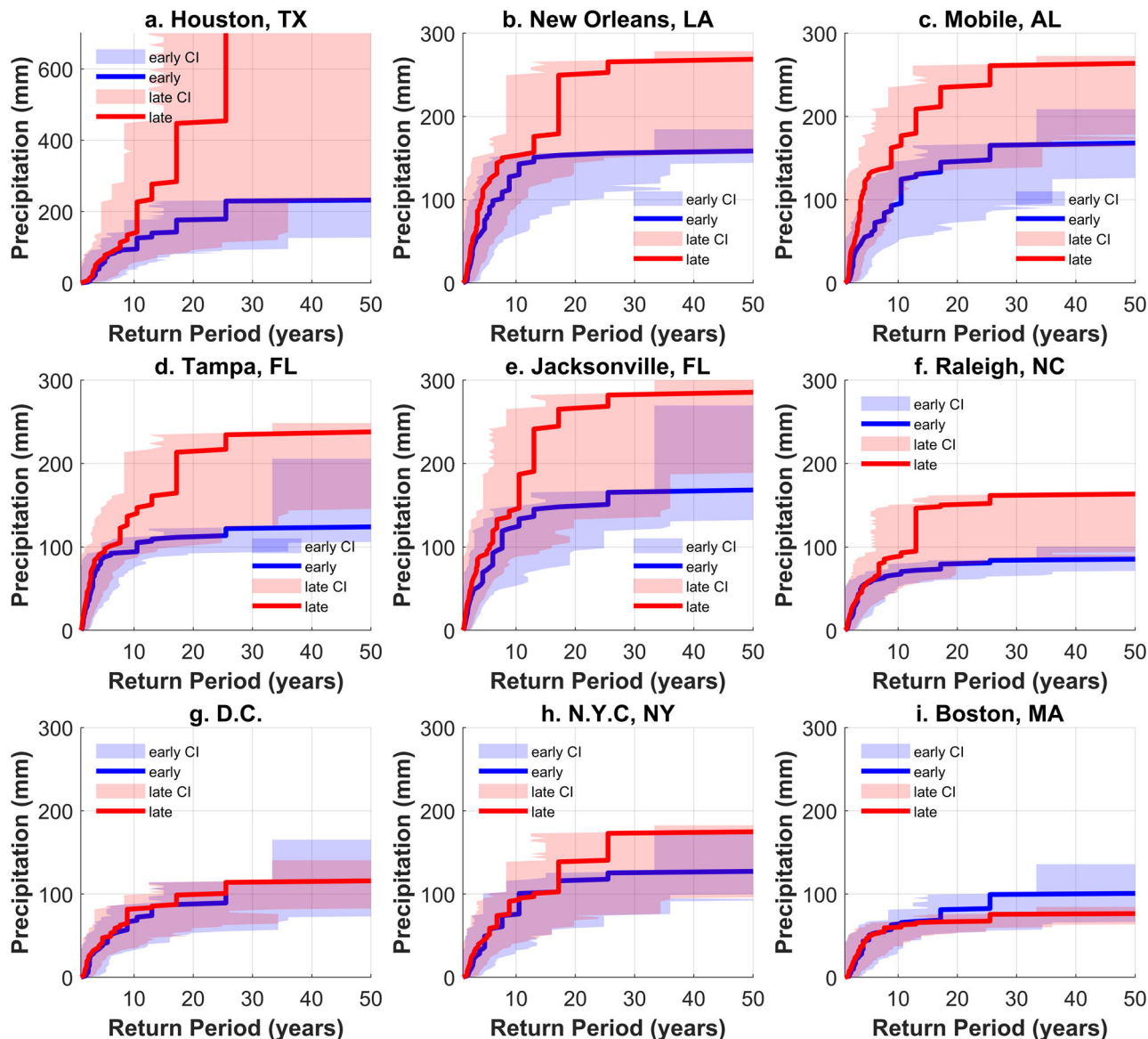


Fig. 3 Return Period (RP) for event Tropical Cyclone Precipitation (TCP) calculated for U.S. cities by the empirical kernel density function of exceedance probability. Each panel represents: **a** Houston, TX. **b** New Orleans, LA. **c** Mobile, AL. **d** Tampa, FL. **e** Jacksonville, FL. **f** Raleigh, NC. **g** District of Columbia, D.C. **h** New York City, N.Y.C., NY. **i** Boston, MA. Confidence Intervals (CI) are estimated by the upper (95%) and lower (5%) boundaries of the Poisson distribution.

prone to TC-related disasters because of their proximity to the ocean. We created a TCP socio-economic exposure index (TCPEI, see data and methods for details) by combining demographic and economic data with physical TCP risk. The TCPEI quantifies how socio-economic exposure to extreme TCP events has changed between the early period (1949–1998) and the late period (1969–2018). There is a general increase in TCPEI from the early period (Fig. 4a, c) to the late period (Fig. 4b, d). About 55 million people were exposed to > 100 mm TCP in the early period, and it increased to 107 million people (92% relative increase) in the late period (Fig. 4c, d). The population with > 1 TCPEI (the highest category for TCP > 200 mm, Fig. 4g) has increased from zero to 4 million. Meanwhile, the population with > 0 TCPEI (lowest category for TCP > 200 mm) has risen ~6 folds from 4.9 million to 29 million. This pattern indicates that the densely populated areas are experiencing more relative increases in exposure to more extreme TCP events.

We also observe significant changes in TCPEI regionally. By averaging the TCPEI within state boundaries, we demonstrate that most states have experienced increases in the median TCPEI, but the magnitude varies from state to state (Supplementary Fig. 11). Louisiana, Florida, and North Carolina have the largest absolute increases (0.49 to 0.70 in median) and relative increases (97 to 100%) in population exposure for > 100 mm TCP (Supplementary Fig. 11a, b). Louisiana, Florida, and Texas have the largest increases in population exposure to >200 mm TCP (0.19 to 0.29 increases in the median with 39 to 58% relative increases, Supplementary Fig. 11c, d). This pattern indicates that states with larger populations are experiencing significantly elevated exposures to extreme TCP events. Florida, Texas, and North Carolina rank high in the relative population growth from 1990 to 2020 (Supplementary Fig. 12). Louisiana has slower population growth, so its significant increase in population exposure is primarily due to elevated physical TCP risk.

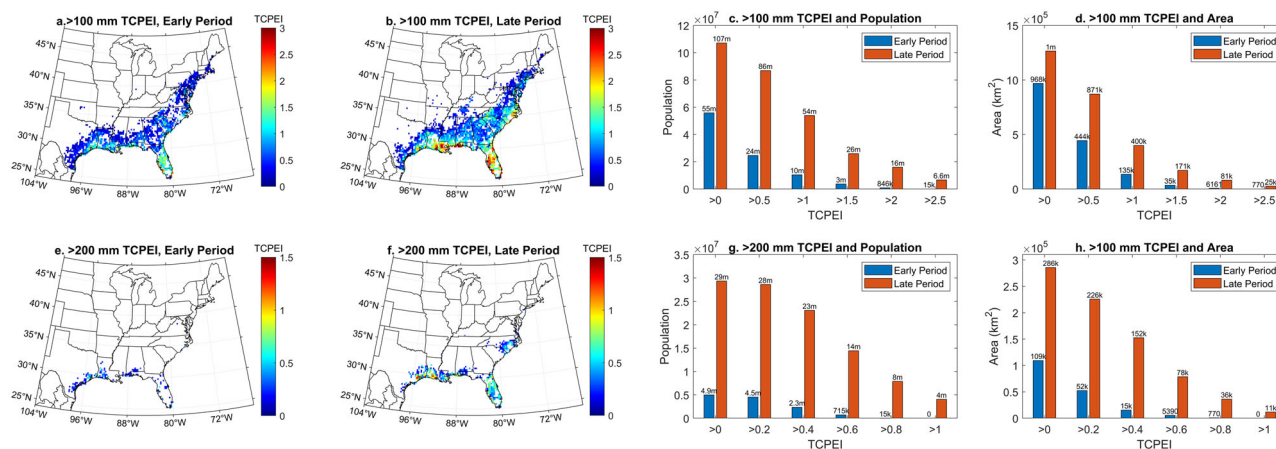


Fig. 4 Spatial Changes in the population-based Tropical Cyclone Precipitation Exposure Index (TCPEI), comparison of population and area for different ranges of TCPEI, relative changes in TCP probabilities, and relative changes in population and Gross Domestic Product (GDP). Each panel represents: **a** >100 mm daily TCPEI in the early period, **b** >100 mm daily TCPEI in the late period, **c** population comparison between the early period and the late period for different ranges of >100 mm daily TCPEI, **d** comparison of the impacted area between the early period and the late period for different ranges of >100 mm daily TCPEI, **e** >200 mm daily TCPEI in the early period, **f** >200 mm daily TCPEI in the late period, **g** population comparison between the early period and the late period for different ranges of >200 mm daily TCPEI, **h** the comparison of the impacted area between the early period and the late period for different ranges >200 mm daily TCPEI, **i** relative changes in >100 mm daily TCP probability, **j** relative changes in >200 mm daily TCP probability, **k** relative changes in the logarithm of the population, **l** relative changes in the logarithm of GDP. The 1970 Population and the 1949–1998 TCP are used to calculate the early period TCPEI. The 2020 population and 1969–2018 TCP are used to calculate the late period TCPEI. In panels **c**, **d**, **g**, **h**, “m” stands for million and “k” stands for thousands.

Economic activities are closely associated with population changes and can be substantially disturbed by extreme weather events like TCs. Similar to the population TCPEI, we have found substantial increases in the exposure of economic activities to extreme TCP events (Supplementary Fig. 13). There are expansions of areas with high TCPEI in the late period (Supplementary Fig. 13b, f) compared with the early period (Supplementary Fig. 13a, e). The > 200 mm TCPEI has more significant relative increases than the >100 mm TCPEI. For example, the GDP exposed to > 100 mm TCP increased by 2%, from \$5.2 trillion to \$5.3 trillion (Supplementary Fig. 13c). Meanwhile, the GDP exposed to >200 mm TCP increased by 124%, from \$581 billion to \$1.3 trillion (Supplementary Fig. 13g). Most states had increases in median GDP TCPEIs (Supplementary Fig. 14), and the southern states had more pronounced relative increases. For example, Florida, Mississippi, Texas, Alabama, and Louisiana rank as the top 5 states highest relative increase (32–131%) in the 200 mm TCPEI (Supplementary Fig. 14c, d).

The TCPEI combines physical TCP risk and socioeconomic information. The TCP risk has larger relative increase (> 60% at many locations, Fig. 4i, j) than the population (<20% at many locations in the southern U.S., Fig. 4k) and GDP (<10% at most locations, Fig. 4l). Therefore, the increase of physical TCP is the major driver of increasing TCPEI over the CONUS. On the other hand, the changes in population/GDP intensified (attenuated) the regional TCPEI changes (e.g., in the southern U.S., Fig. 4a, b), with major influences from the changing physical TCP risk.

Discussion

Large areas in the southern U.S. and coastal mid-Atlantic have significant positive trends in annual total TCP and maximum event TCP during the last 70 years. Widespread increases in TCP probability occur in coastal regions and they are most pronounced in the southern U.S. Elevated TCP risk is also observed in most coastal cities. Those changes in physical TCP risk are associated with increased TCP rain rates and decreased TC translation speed^{16,41}. Our records also show that the most

significant decreases in TC translation speed are in the slowest moving TCs (<20 knots, Supplementary Fig. 8a) and in TCs tracking towards the northwest (Supplementary Fig. 8b). Large spatial variabilities also exist in the temporal trend in TCP. These variabilities are a result of multiple factors, including anthropogenic climate change^{3,41,42}, natural variability (e.g., El Niño–Southern Oscillation and Atlantic Multidecadal Variability) and forcing from volcanic activity^{28,43,44}, and inconsistencies and limitations of historical observations²⁰. Therefore, we need more high-quality and long-term historical TCP data and carefully controlled numerical experiments for a better understanding of changes in TCP and its relationship with climate/environment.

Many previous studies showed increasing risk of extreme weather events under anthropogenic climate change^{3,45,46}. Some provide quantitative estimates of social exposure to extreme heat and cold events, floods, sea level rise, etc.^{47–50}. Using the TCP data, we proposed a new index that combines changes in the physical probability of extreme events and socioeconomic measurements directly affected by the disaster. We demonstrated that while the physical TCP risk is the primary driver determining the socioeconomic exposures, increases in population and GDP are exacerbating these changes. Areas with high TCPEI have expanded substantially due to rapid urbanization and population growth in the southern and mid-Atlantic states of CONUS during the last 70 years (Fig. 4k, l and Supplementary Fig. 15). Future regional population growth⁵¹ and urbanization⁵² may intensify TCP flooding^{6,33} and its societal exposure. In addition, the spatial heterogeneity in the population growth and economic development cause differences in local exposure to TCP hazards. Potential damage may increase exponentially due to changes in the magnitude and frequency of extreme TC events^{53,54}. Compound events such as storm surge and pluvial floods can intensify those damages⁵⁵. At the local level, government and citizens need more detailed mitigation strategies such as updated building codes, expanded insurance, and infrastructure hardening¹¹ when faced with increased exposure to extreme TCP. Our research quantifies how physical risk from TCP and societal exposure changed simultaneously across CONUS during the last 70 years.

Geiger et al.¹⁴ predict an annual global exposure increase of 26% (33 million people) to TC winds for every 1 °C rise in global mean surface temperature. We demonstrated that the number of people exposed to >200 mm TCP has increased by 24 million (489% relative increase, Fig. 4g) and the GDP exposure to >200 mm TCP has increased by \$719 billion (124% relative increase, Supplementary Fig. 10g). Future research needs to address how compound flood⁵⁶ exposure (extreme floods generated by both rainfall and storm surge) changes by integrating and coupling earth system models, hydrological/hydraulic models, and socio-economic/land cover change models. Substantial disparities exist in social exposure^{57,58} to TC hazards, and our TCPEI does not explicitly address this. Future metrics of social exposure to extreme weather events also need to reflect social disparity so the most vulnerable social groups to nature disasters can be better protected.

Data and methods

Precipitation data are from the Daily Global Historical Climatology Network (GHCN-D), which provides a complete global daily precipitation record. They are freely accessible from National Centers for Environmental Information, NCEI (<https://www.ncei.noaa.gov/products/land-based-station/global-historical-climatology-network-daily>). We obtained daily precipitation observations for TCP calculation from GHCN-D gauges that are within a moving daily boundary. Four connected circles define this daily boundary with 600 km radius to four TC centers recorded at 6 h intervals from the International Best Track Archive for Climate Stewardship (IBTrACS). Here a larger radius (600 km) is used instead of 500 km to extract rain gauges because we want to avoid missing the rain gauge observations outside the boundary when spatial interpolation is processed near the 500 km boundary. The IBTrACS data are also freely available from NCEI (<https://www.ncdc.noaa.gov/ibtracs/>). After a wind under-catch bias correction²⁰, we use Inverse Distance Weighting (IDW) interpolation⁵⁹ to estimate the precipitation at a set of grid points with even spacing of 0.25° across the CONUS:

$$P_g = \left[\sum_{i=1}^N (d_i)^{-u} z_i \right] / \left[\sum_{i=1}^N (d_i)^{-u} \right] \quad (1)$$

P_g is the precipitation estimation at each grid point. N is the number of gauges within a searching distance ($R = 30$ km) for each grid point. d_i is the distance from each gauge to a specific grid within R . u is the weighting power and is set to 2 as the default value. After we calculate P_g for all daily TCP, only grids within 500 km of the storm track finally enter our daily TCP database. We choose the 500 km boundary because it provides consistent criteria for our 70-year record to define TCP. It also includes most precipitation systems in TC^{41,60}, including both convective precipitation in the core and stratiform precipitation in outer bands. This routine has been validated and optimized by comparing available TMPA observations²⁰ and is available upon request. To guarantee the consistency of the data, we only chose grids with at least one consistent gauge with 70 years of complete observations within R (30 km). We have chosen 4816 grids (Supplementary Fig. 1) based on that criterion, and most have more than two gauges within 30 km, which guarantees there are no missing observations in the time series. Therefore, we believe that the final grids (4816) provide good spatial coverage of the TCP's affected areas across the CONUS.

The population for 1970 is from The Global Population Density Grid Time Series v1 and the 2020 population is from the Gridded Population of the World (GPW) v4. They are compiled by the Socioeconomic Data and Application Center (SEDAC) of Columbia University both have 1 km spatial resolution. GDP data

at 1 km resolution are obtained for 1990 and 2015 from the Gridded global datasets for Gross Domestic Product and Human Development Index from 1990 to 2015²². We re-scaled the population and GDP data for each 0.25° grid by summing all 1 km grid values within each TCP grid box.

We then aggregate daily TCP observations at each grid into event TCP based on the duration of each TC (from the start to the end of each TC event over CONUS) and sum total TCP in each year as the annual total TCP. A 70-year climatology is constructed for annual total TCP, annual maximum event TCP, and annual maximum daily TCP at each grid. The Mann–Kendall non-parametric test^{61,62} is used to detect trends in those time series and the Sen's slope⁶³ is calculated for each time series. We use a 95% significance level for both non-parametric methods for all trend detections. We also calculate return periods for daily and event TCP samples at each grid by constructing empirical exceedance probability density⁶⁴. For any sample of TCP observations (event or daily) at a specific grid, the non-parametric kernel density estimation (KDE) function is defined as:

$$\hat{f}_h(p) = \frac{1}{nh} \sum_{i=1}^n K\left(\frac{p - p_i}{h}\right) \quad (2)$$

where p_1, p_2, \dots, p_n are observations of TCP at each grid with an unknown distribution; n is the sample size. h is the bandwidth set as 0.02 to provide enough detail for each KDE curve. K is the kernel smoothing function, which we used a Gaussian kernel smoother, expressed as:

$$K(p^*, p_i) = \exp\left(-\frac{(p^* - p_i)^2}{2\sigma^2}\right) \quad (3)$$

where σ is the length scale for the input space. After a KDE curve is fitted, we can estimate the cumulative distribution function (CDF) and the Exceedance Probability Function (EPF) ($1 - \text{CDF}$). By using a linear interpolation approach⁶⁵, we can find the Return Period (RP) estimate for each TCP threshold (e.g., > 100 mm). We estimated the RPs of daily and event TCP thresholds for all 4816 grids and compared the estimates from the early period (1949–1998) to the late period (1969–2018). We did not make extrapolations, so our most extended return period is 50 years. We removed all locations where we could not determine a value from this empirical EPF calculation. We also assume both the event and daily TCP at each location follow a Poisson Distribution^{6,66} and use it to calculate Confidence Intervals (CI) by the upper 95% and lower 5% boundary for each kernel. Finally, we compare the spatial distribution of RP for different magnitudes of TCP between the early and late periods and demonstrate how the whole TCP probability profile changes at night cities in the CONUS. We also finished a sensitivity analysis that compares two non-overlapping periods of 35 years (Supplementary Fig. 10). Results show that there is little change in the pattern of TCP RP change as compared to the overlapping test in Fig. 3. The long tails of the distribution for extreme values have systematically shifted to a shorter RP. Therefore, the RP estimated with a longer period of record (Fig. 3) will have less uncertainty in the estimates of extreme values.

To quantify society's exposure to extreme TCP events, we created a TCP exposure index (TCPEI):

$$\text{TCPEI} = \frac{\log_{10} \text{SEC}}{\text{RP}} \quad (4)$$

Where the SEC stands for Social Economic Criteria, in this study, we utilized two datasets: population and annual GDP in U.S. Dollars (\$). We use the logarithm of 10 for the SEC to re-scale the population and GDP for spatial analysis. The RP is the Return Period for a specific magnitude of TCP (e.g., 100 mm). The TCPEI increases as population or GDP increases or RP becomes

shorter (higher physical TCP risk). Since there can be spatial and temporal changes in both physical TCP risk and population/socio-economic activities, our TCPEI can quantify the spatial variability of socio-economic exposure and identify hot spots vulnerable to TC floods. Supplementary Fig. 16 shows a flowchart that summarizes all data processing and analysis used for this study.

Data availability

All data used in this study is available at Zenodo at: <https://doi.org/10.5281/zenodo.7292939>.

Code availability

All codes used in this study are available at Zenodo at: <https://doi.org/10.5281/zenodo.7292939>. Matlab 2021 was used to analyze the data and generate graphics.

Received: 11 August 2022; Accepted: 18 November 2022;

Published online: 10 December 2022

References

- NOAA. National Centers for Environmental Information (NCEI) *U.S. Billion-Dollar Weather and Climate Disasters* (2022). <https://www.ncei.noaa.gov/access/billions/>, <https://doi.org/10.25921/stkw-7w73>. Accessed 1 June 2022.
- Emanuel, K. Assessing the present and future probability of Hurricane Harvey's rainfall. *Proc. Natl Acad. Sci. USA* **114**, 12681–12684 (2017).
- Knutson, T. et al. Tropical cyclones and climate change assessment: Part II: Projected response to anthropogenic warming. *Bull. Am. Meteorol. Soc.* **101**, E303–E322 (2020).
- Patricola, C. M. & Wehner, M. F. Anthropogenic influences on major tropical cyclone events. *Nature* **563**, 339–346 (2018).
- Hall, T. M. & Kossin, J. P. Hurricane stalling along the North American coast and implications for rainfall. *npj Clim. Atmos. Sci.* <https://doi.org/10.1038/s41612-019-0074-8> (2019).
- Zhu, L., Emanuel, K. & Quiring, S. M. Elevated risk of tropical cyclone precipitation and pluvial flood in Houston under global warming. *Environ. Res. Lett.* **16**, 094030 (2021).
- Dixon, P. G. & Mote, T. L. Patterns and causes of Atlanta's urban heat island-initiated precipitation. *J. Appl. Meteorol.* **42**, 1273–1284 (2003).
- Pan, B. et al. Determinant role of aerosols from industrial sources in Hurricane Harvey's catastrophe. *Geophys. Res. Lett.* <https://doi.org/10.1029/2020gl090014> (2020).
- Roson, R. & Mensbrugge, D. V. D. Climate change and economic growth: impacts and interactions. *Int. J. Sustain. Econ.* **4**, 270 (2012).
- Pielke, R. A. et al. Normalized hurricane damage in the United States: 1900–2013;2005. *Nat. Hazards Rev.* **9**, 29–42 (2008).
- Klotzbach, P. J., Bowen, S. G., Pielke, R. & Bell, M. Continental U.S. hurricane landfall frequency and associated damage: observations and future risks. *Bull. Am. Meteorol. Soc.* **99**, 1359–1376 (2018).
- Grinsted, A., Ditlevsen, P. & Christensen, J. H. Normalized US hurricane damage estimates using area of total destruction, 1900–2018. *Proc. Natl Acad. Sci. USA* **116**, 23942–23946 (2019).
- Weinkle, J. et al. Normalized hurricane damage in the continental United States 1900–2017. *Nat. Sustainability* **1**, 808–813 (2018).
- Geiger, T., Gütschow, J., Bresch, D. N., Emanuel, K. & Frieler, K. Double benefit of limiting global warming for tropical cyclone exposure. *Nat. Clim. Change* **11**, 861–866 (2021).
- Pielke, R. A. Are there trends in hurricane destruction? *Nature* **438**, E11–E11 (2005).
- Peduzzi, P. et al. Global trends in tropical cyclone risk. *Nat. Clim. Change* **2**, 289–294 (2012).
- Ye, M., Wu, J., Liu, W., He, X. & Wang, C. Dependence of tropical cyclone damage on maximum wind speed and socioeconomic factors. *Environ. Res. Lett.* **15**, 094061 (2020).
- Tonn, G. & Czajkowski, J. US tropical cyclone flood risk: storm surge versus freshwater. *Risk Analysis* <https://doi.org/10.1111/risa.13890> (2022).
- Cutter, S. et al. in *Managing the Risks of Extreme Events and Disasters to Advance Climate Change Adaptation: Special Report of the Intergovernmental Panel on Climate Change* (eds Field, C. B., Dahe, Q., Stocker, T. F. & Barros, V.) 291–338 (Cambridge University Press, 2012).
- Zhu, L. & Quiring, S. M. An extraction method for long-term tropical cyclone precipitation from daily rain gauges. *J. Hydrometeorol.* **18**, 2559–2576 (2017).
- Center for International Earth Science Information Network - CIESIN - Columbia University. 2016. Gridded Population of the World, Version 4 (GPWv4): Administrative Unit Center Points with Population Estimates. Palisades, NY: NASA Socioeconomic Data and Applications Center (SEDAC). <https://doi.org/10.7927/H4F47M2C>. Accessed 1 June 2022.
- Kummu, M., Taka, M. & Guillaume, J. H. A. Gridded global datasets for Gross Domestic Product and Human Development Index over 1990–2015. *Scientific Data* **5**, 180004 (2018).
- Kunkel, K. E. et al. Meteorological causes of the secular variations in observed extreme precipitation events for the conterminous United States. *J. Hydrometeorol.* **13**, 1131–1141 (2012).
- Knight, D. B. & Davis, R. E. Climatology of tropical cyclone rainfall in the Southeastern United States. *Phys. Geogr.* **28**, 126–147 (2007).
- Knight, D. B. & Davis, R. E. Contribution of tropical cyclones to extreme rainfall events in the southeastern United States. *J. Geophys. Res.* <https://doi.org/10.1029/2009jd012511> (2009).
- Nogueira, R. C. & Keim, B. D. Annual volume and area variations in tropical cyclone rainfall over the Eastern United States. *J. Climate* **23**, 4363–4374 (2010).
- Aryal, Y. N., Villarini, G., Zhang, W. & Vecchi, G. A. Long term changes in flooding and heavy rainfall associated with North Atlantic tropical cyclones: roles of the North Atlantic Oscillation and El Niño-Southern Oscillation. *J. Hydrology* **559**, 698–710 (2018).
- Bregy, J. C. et al. Spatiotemporal variability of tropical cyclone precipitation using a high-resolution, gridded (0.25° × 0.25°) dataset for the Eastern United States, 1948–2015. *J. Climate* **33**, 1803–1819 (2020).
- Easterling, D. R. et al. Climate extremes: observations, modeling, and impacts. *Science* **289**, 2068–2074 (2000).
- Cloux, S., Garaboa-Paz, D., Insua-Costa, D., Míguez-Macho, G. & Pérez-Muñuzuri, V. Extreme precipitation events in the Mediterranean area: contrasting two different models for moisture source identification. *Hydrol. Earth Syst. Sci.* **25**, 6465–6477 (2021).
- Roca, R. & Fiolleau, T. Extreme precipitation in the tropics is closely associated with long-lived convective systems. *Commun. Earth Environ.* <https://doi.org/10.1038/s43247-020-00015-4> (2020).
- Tuholske, C. et al. Global urban population exposure to extreme heat. *Proc. Natl Acad. Sci. USA* **118**, e2024792118 (2021).
- Zhang, W., Villarini, G., Vecchi, G. A. & Smith, J. A. Urbanization exacerbated the rainfall and flooding caused by hurricane Harvey in Houston. *Nature* **563**, 384–388 (2018).
- Zhu, L., Quiring, S. M., Guneralp, I. & Peacock, W. G. Variations in tropical cyclone-related discharge in four watersheds near Houston, Texas. *Clim. Risk Manage.* **7**, 1–10 (2015).
- O'Gorman, P. A. & Schneider, T. The physical basis for increases in precipitation extremes in simulations of 21st-century climate change. *Proc. Natl Acad. Sci. USA* **106**, 14773–14777 (2009).
- Trenberth, K. E., Dai, A., Rasmussen, R. M. & Parsons, D. B. The changing character of precipitation. *Bull. Am. Meteorol. Soc.* **84**, 1205–1218 (2003).
- Kossin, J. P. A global slowdown of tropical-cyclone translation speed. *Nature* **558**, 104–107 (2018).
- Lanzante, J. R. Uncertainties in tropical-cyclone translation speed. *Nature* **570**, E6–E15 (2019).
- Yamaguchi, M., Chan, J. C. L., Moon, I.-J., Yoshida, K. & Mizuta, R. Global warming changes tropical cyclone translation speed. *Nat. Commun.* <https://doi.org/10.1038/s41467-019-13902-y> (2020).
- Glaeser, E. L. & Tobio, K. The Rise of the Sunbelt. *National Bureau of Economic Research Working Paper Series* No. 13071, <https://doi.org/10.3386/w13071> (2007).
- Guzman, O. & Jiang, H. Global increase in tropical cyclone rain rate. *Nat. Commun.* <https://doi.org/10.1038/s41467-021-25685-2> (2021).
- Maxwell, J. T. et al. Recent increases in tropical cyclone precipitation extremes over the US east coast. *Proc. Natl Acad. Sci. USA* **118**, e2105636118 (2021).
- Bregy, J. C. et al. US Gulf Coast tropical cyclone precipitation influenced by volcanism and the North Atlantic subtropical high. *Commun. Earth Environ.* <https://doi.org/10.1038/s43247-022-00494-7> (2022).
- Moon, I.-J., Kim, S.-H. & Chan, J. C. L. Climate change and tropical cyclone trend. *Nature* **570**, E3–E5 (2019).
- AghaKouchak, A. et al. *Annual Review of Earth and Planetary Sciences* (eds Jeanloz, R. & Freeman, K. H.) Vol. 48, 519–548 (Annual Reviews, 2020).
- Min, S.-K., Zhang, X., Zwiers, F. W. & Hegerl, G. C. Human contribution to more-intense precipitation extremes. *Nature* **470**, 378–381 (2011).
- Paprotny, D., Morales-Nápoles, O. & Jonkman, S. N. HANZE: a pan-European database of exposure to natural hazards and damaging historical floods since 1870. *Earth Syst. Sci. Data* **10**, 565–581 (2018).

48. Ho, H. C. et al. Spatiotemporal influence of temperature, air quality, and urban environment on cause-specific mortality during hazy days. *Environ. Int.* **112**, 10–22 (2018).
49. Smid, M., Russo, S., Costa, A. C., Granell, C. & Pebesma, E. Ranking European capitals by exposure to heat waves and cold waves. *Urban Clim.* **27**, 388–402 (2019).
50. Dasgupta, S., Laplante, B., Murray, S. & Wheeler, D. Exposure of developing countries to sea-level rise and storm surges. *Climatic Change* **106**, 567–579 (2011).
51. Vespa, J. A., Medina, L. & Armstrong, M. A. Demographic turning points for the United States: population projections for 2020 to 2060, Population Estimates and Projections, Current Population Reports (2018). <https://www.census.gov/library/publications/2020/demo/p25-1144.html>. Accessed 1 June 2022.
52. Angel, S., Parent, J., Civco, D. L., Blei, A. & Potere, D. The dimensions of global urban expansion: estimates and projections for all countries, 2000–2050. *Prog. Planning* **75**, 53–107 (2011).
53. Emanuel, K. Response of global tropical cyclone activity to increasing CO₂: results from downscaling CMIP6 models. *J. Climate* **34**, 57–70 (2021).
54. Wang, S. & Toumi, R. More tropical cyclones are striking coasts with major intensities at landfall. *Sci. Rep.* <https://doi.org/10.1038/s41598-022-09287-6> (2022).
55. Gori, A., Lin, N., Xi, D. & Emanuel, K. Tropical cyclone climatology change greatly exacerbates US extreme rainfall–surge hazard. *Nature Climate Change* **12**, 171–178 (2022).
56. Gori, A., Lin, N. & Xi, D. Tropical cyclone compound flood hazard assessment: from investigating drivers to quantifying extreme water levels. *Earth's Future* <https://doi.org/10.1029/2020ef001660> (2020).
57. Parks, R. M. et al. Tropical cyclone exposure is associated with increased hospitalization rates in older adults. *Nat. Commun.* <https://doi.org/10.1038/s41467-021-21777-1> (2021).
58. Cutter, S., Schumann, R. & Emrich, C. Exposure, social vulnerability and recovery disparities in New Jersey after Hurricane Sandy. *J. Extreme Events* **01**, 1450002 (2014).
59. Shepard, D. *A Two-Dimensional Interpolation Function for Irregularly-Spaced Data* (ACM Press).
60. Nogueira, R. C. & Keim, B. D. Contributions of Atlantic tropical cyclones to monthly and seasonal rainfall in the eastern United States 1960–2007. *Theor. Appl. Climatol.* **103**, 213–227 (2011).
61. Mann, H. B. Nonparametric tests against trend. *Econometrica* **13**, 245–259 (1945).
62. Kendall, M. G. *Rank Correlation Methods* (Griffin, 1975).
63. Sen, P. K. Estimates of the regression coefficient based on Kendall's Tau. *J. Am. Stat. Assoc.* **63**, 1379–1389 (1968).
64. Bowman, A. W. & Azzalini, A. Applied smoothing techniques for data analysis: the kernel approach with S-plus illustrations. *J. Am. Stat. Assoc.* **94**, 982 (1999).
65. Akima, H. A new method of interpolation and smooth curve fitting based on local procedures. *J. ACM* **17**, 589–602 (1970).
66. Zhu, L., Quiring, S. M. & Emanuel, K. A. Estimating tropical cyclone precipitation risk in Texas. *Geophysical Research Letters* **40**, 6225–6230 (2013).

Acknowledgements

L.Z. is supported by the Faculty Research and Creative Activities Award (FRACAA) and the Lucia Harrison Endowment Funding by Western Michigan University. S.Q. is supported by the Translational Data Analytics Institute and The Ohio State University.

Author contributions

L.Z. conceptualized and designed the research. L.Z. executed the data analysis and drafted the manuscript. S.Q. provided feedback on the research design and helped to edit the manuscript.

Competing interests

The authors declare no competing interests.

Additional information

Supplementary information The online version contains supplementary material available at <https://doi.org/10.1038/s43247-022-00639-8>.

Correspondence and requests for materials should be addressed to Steven M. Quiring.

Peer review information *Communications Earth & Environment* thanks Justin Maxwell and the other, anonymous, reviewer(s) for their contribution to the peer review of this work. Primary Handling Editors: Aliénor Lavergne. Peer reviewer reports are available.

Reprints and permission information is available at <http://www.nature.com/reprints>

Publisher's note Springer Nature remains neutral with regard to jurisdictional claims in published maps and institutional affiliations.



Open Access This article is licensed under a Creative Commons Attribution 4.0 International License, which permits use, sharing, adaptation, distribution and reproduction in any medium or format, as long as you give appropriate credit to the original author(s) and the source, provide a link to the Creative Commons license, and indicate if changes were made. The images or other third party material in this article are included in the article's Creative Commons license, unless indicated otherwise in a credit line to the material. If material is not included in the article's Creative Commons license and your intended use is not permitted by statutory regulation or exceeds the permitted use, you will need to obtain permission directly from the copyright holder. To view a copy of this license, visit <http://creativecommons.org/licenses/by/4.0/>.

© The Author(s) 2022